TECHNICAL PAPER

Evaluation of different tool geometries in the finite element simulation of ultrasonic-assisted drilling of Ti6A14V

Peng Wang[1] · Dazhong Wang[1]

Abstract
This paper attempts to analyze the effect of various drilling parameters such as feed rate, spindle speed and vibration frequency on performance characteristics such as thrust force, effective stresses, temperature and chip morphology in conventional drilling (CD) and ultrasonic-assisted drilling (UAD) of Ti6A14V using three different point angle (140°, 120°, 90°) drill bits in order to optimize the chip breakability of Ti6A14V. The three different point angle drill bits are utilized to establish the finite element models (FEM) to simulate the drilling process with Lagrangian approach in DEFORM-3D software. The simulations are validated by the experimental findings and analytical data of thrust forces, and the percent errors in results range approximately between 3 and 7%. The results obtained prove that UAD can produce segmental discontinuous chip, lower thrust force, lower process temperature and lower effective stress. The point angle of 120° drill achieved the thinnest chip thickness and the excellent effects of chip breaking. The achieved results are assumed to help for the optimization of the drill tool geometries, drilling parameters and chip breakability.

Keywords Ultrasonic-assisted drilling · Point angle drill bits · Chip breakability · Chip morphology

1 Introduction

The productivity of the drilling process is so important that it is generally performed at the end of machining sequence [1]. It accounts for 40% of all the material removal processes [2]. Ti6Al4V is widely used in aerospace, automotive, biomedical engineering, bone transplantation and chemical industry [3] for bone replenishment and low elastic modulus [4, 5] due to its high strength to weight ratio, low density, corrosion resistance, wear resistance and other good mechanical properties. Although the surface of Ti6Al4V has good workability from the viewpoint of cutting force, its inherent characteristics, especially low thermal conductivity, relatively low modulus of elasticity, high temperature strength, high chemical activity and small deformation coefficient [6–8], lead to Ti6Al4V difficult to process and often require relatively long processing times and expensive tools [9].

In recent years, many researchers have experimentally carried out a large amount of research during CD Ti6Al4V with respect to thrust force, torque and hole quality. Arrazola et al. [10] have reported through extensive experimental studies under various processing conditions that titanium alloys have poor processability. Islam et al. [11] proposed a transient heat distribution coefficient model between the chip and the rake face of the tool to further improve the understanding of thermomechanical phenomena. Abdelhafeez et al. [12] carried out an experimental design based on response surface method to determine the impact of cutting speed and feed rate on burr size, hole diameter and roundness as well as the wear of tool surface behind the tool in Ti6Al4V drilling. Pawar et al. [13], respectively, compared the wear of coated cemented carbide drill bits in Ti, CFRP and CFRP/Ti-laminated drilling, and analyzed the impact of chip flow on the hole surface quality. Rahim and Sasahara [14] compared thrust and coolant–lubricant conditions at a cutting speed of 60 m/min and a feed rate of 0.1 mm/rev. The results show that compared with other coolant–lubricant conditions, blowing condition generated the maximum thrust when the feed rate increases, and the thrust and torque values increase significantly. Liu et al. [15] conducted a series of experiments to study the chip

✉ Dazhong Wang
  wdzh168@126.com

[1] Shanghai University of Engineering Science, 333 Longteng Road, Shanghai 201620, China

morphology and performance of aluminum and titanium laminates drilled using the double-cone bit. They found that the double-cone bit easily deforms the chip morphology and produces funnel-shaped chips. In the drilling process, tool geometry plays an important role in hole quality [16]. Zhang et al. [17] proposed an improved theoretical force model that takes into account material removal and plastic accumulation mechanisms. Kuo et al. [18] developed a single-step drilling technique for stacking multilayer metal composites using uncoated and PVD-coated carbide drills. The results show that the uncoated carbide drill bit has a sharper cutting radius (higher sharpness), and the tool wear is more serious than the PVD-coated carbide drill bit.

CD processing generally produces higher cutting forces. This increase in value reduces tool life and surface quality [19]. In recent years, ultrasonic-assisted cutting as a new processing method has been found to be very effective in processing difficult-to-machine materials [20, 21]. UAD is a non-traditional hybrid processing technology that combines the characteristics of traditional drilling and vibration processing techniques to significantly improve the machinability of advanced difficult-to-machine materials [22]. This periodic interrupted cut produced a series of improvements during the drilling process, and some researchers conducted experimental analyses [23]. Yang et al. [24] analyzed the critical maximum undeformed equivalent chip thickness for ductile–brittle transition of zirconia ceramics under different lubrication conditions. Pujana et al. [20] analyzed the UAD of Ti6Al4V, but applied vibration to the workpiece rather than applying it to the drill bit. Barani et al. [25] studied the effect of longitudinal vibration on the drilling of Al2024T6. They obtained a better machined surface than the CD due to the lower surfacing edge of the UAD. Amini et al. [26] found that the thrust force was reduced by 70% in UAD, and the continuous chips became discontinuous in CD. Sanda et al. [27] concluded that UAD has lower cutting forces and better surface gloss than CD.

Although a large number of experimental studies have been conducted on the application of ultrasonic vibration in the drilling process, a large amount of work is required in order to realize the industrialization and high-efficiency application of the technology [23]. For the study of machining processes, experimental research is costly and time-consuming, especially when multiple parameters are integrated. In addition to the experimental methods, numerical methods are also used for simulation. The most commonly used numerical technique in metal cutting is finite element modeling [28]. Muhammad et al. [29] developed a three-dimensional finite element model of the drilling process using DEFORM-3D. They used the finite element model to study the effects of external heat sources on thrust force and torque of drill bit, and demonstrated the advantages of titanium alloy hot drills in reducing

thrust force and torque. Wu et al. [30] used a simplified idealized three-dimensional finite element model to analyze the drilling process of titanium alloy Ti6Al4V and predicted its drilling force. Marasi [31] established a two-dimensional model in DEFORM-2D to study the effects of cutting speed and feed rate during the turning process of Ti6Al4V. The experimental run was designed according to the design of experiment (DOE) method. The study has shown that the cutting force increases with increasing cutting speed. Ahmad [32] developed a three-dimensional thermomechanical coupled finite element model for the steel 2080 drilling process and studied the effects of cutting parameters on drill bit temperature, drill life, thrust force and torque. Chatterjee et al. [33] used the harmony search algorithm to optimize the cutting parameters. The roundness error was verified by the finite element method using DEFORM-3D. The hole diameter and temperature will affect the roundness and cylinder, thus affecting the hole characteristics. Micromilling experiments assisted with and without laser oxidation were performed on cemented carbide. They performed thermal prediction, edge establishment and wear calculation using the finite element method and concluded that these parameters depend on the processing parameters [34]. Attanasio et al. [35] simulated tool wear during drilling of Inconel 718. The predicted results agree well with the measured data.

Ucun [36] conducted experimental and numerical simulations on the thrust and torque of aluminum drilling materials. He concluded that there is 80–90% consistency between the simulated data and the experimental data. Phadnis et al. [37] investigated the effect of variation in intensity of ultrasonic energy on the extent of softening in the carbon/epoxy composite for UAD. The results show that the average thrust force of the UAD is reduced by 30% compared to CD. The prediction results are in good agreement with the experimental results.

So far, the research literature on UAD of Ti6Al4V using different point angle drills in the finite element simulation has not yet been reported. Detailed analysis of tool geometry in drilling metal stack is significant lacking. The different point angles may change chip flow direction to facilitate chip flowing and breaking. In this paper, the three different point angle drill bits are utilized to establish the finite element models (FEM) to simulate the drilling process with Lagrangian approach in DEFORM-3D software. This study attempts to analyze the effect of various drilling parameters such as feed rate, spindle speed and vibration frequency on performance characteristics such as thrust force, effective stresses, temperature and chip morphology in CD and UAD of Ti6A14V using three different point angle drill bits in order to optimize the chip break ability of Ti6A14V.

2 3D finite element model of drilling process

2.1 Geometry modeling and meshing

In order to reduce the calculation time, only the drill bit and surrounding part of drill tool were introduced into the drill model. Three different geometrical drills have been employed during these simulations, as shown in Fig. 1:

Drill 1 has a diameter of 3.6 mm, a point angle of 140° and a helix angle of 35°. The length of major cutting edge shorter of a point angle of 140° is shorter. The cutting force generated by major cutting edge can be reduced obviously.

Drill 2 has a diameter of 3.6 mm, a point angle of 120° and a helix angle of 35°. From the point of view of thrust force and back force, the cutting effect of a point angle of 120° is very good.

Drill 3 has a diameter of 3.6 mm, a point angle of 90° and a helix angle of 35°. Due to the longer length of the main cutting edge of a point angle of 90°, the load on the unit cutting edge is reduced, which is effective for the axial stability of the drill bit. The locating performance of drill tip is improved effectively, and the drilling process of hole entrance becomes easier.

The meshing method of the three tools adopts absolute mesh division. The mesh type is tetrahedral mesh, and the mesh is refined at the tool tip. The minimum mesh size is 0.1 mm, the size ratio is 7, and no. of elements is 4748.

Once again to reduce the simulation time, a small cylindrical workpiece 6 mm in diameter and 1.8 mm in thick was created. The meshing method of the workpiece is also divided by absolute mesh. The mesh type is tetrahedral mesh. The mesh of the area where the workpiece and the tool are in contact with each other causes high temperature, and the mesh of the area far away from the cutting edge is automatically divided. The minimum mesh size is 0.04 mm, the size ratio is 7, and no. of elements is 32,520.

Figure 2 shows the prediction model of chip in CD and UAD. It can be seen that the chip morphology in CD is continuous spiral chip, whereas it is discontinuous flaky chip in UAD.

2.2 Material properties and constitutive model

The Johnson–Cook material model [38] in Eq. 1 is applied to define material deformation because the metal cutting is a dynamic process accompanied by large strains, large strain rates and high temperature effects of material.

$$\sigma = (A + B\varepsilon^n)\left(1 + Cln\frac{\dot{\varepsilon}}{\dot{\varepsilon}_0}\right)\left(1 + \left(\frac{T - T_r}{T_m - T_r}\right)^m\right) \quad (1)$$

where σ is equivalent flow stress, ε is equivalent plastic strain, $\dot{\varepsilon}$ is plastic strain rate, T is working temperature, T_r is room temperature, T_m is melting point, and $\dot{\varepsilon}_0$ is the reference strain rate. Parameters A, B, n, C and m are constant coefficients of material. These constants are determined based on Split–Hopkinson bar test and, respectively, are
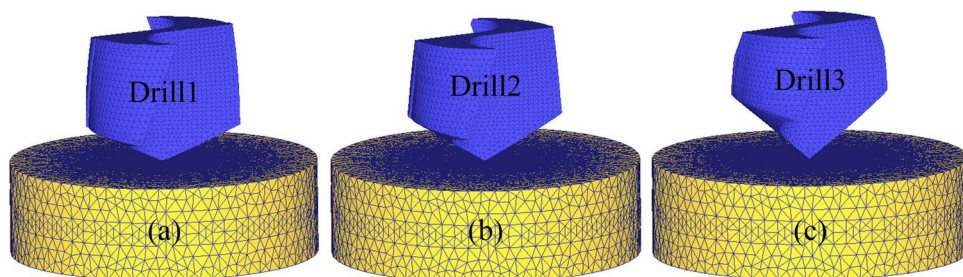
Fig. 1 Simulation modeling

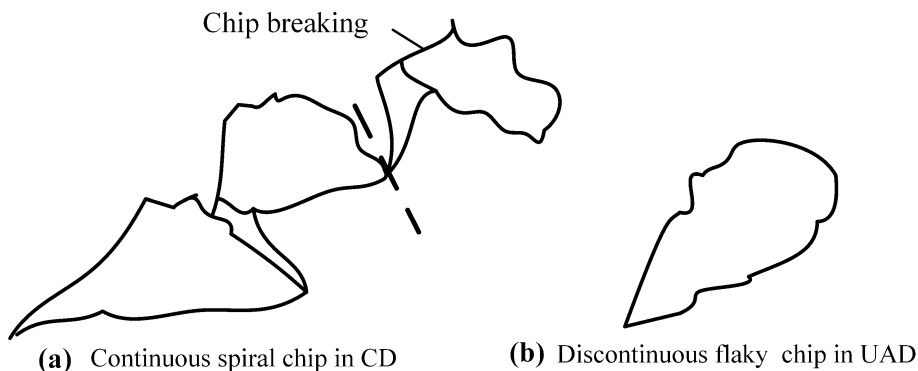

Fig. 2 Chip breakability modeling

(a) Continuous spiral chip in CD   **(b)** Discontinuous flaky chip in UAD

Table 1 Material constants for Ti6A14V [20]

Material	A (MPa)	B (MPa)	n	C	m	$\dot{\varepsilon}$	T_r (°C)	T_m (°C)
Ti6A14V	782.7	498.4	0.28	0.028	1.0	0.001	20	1460
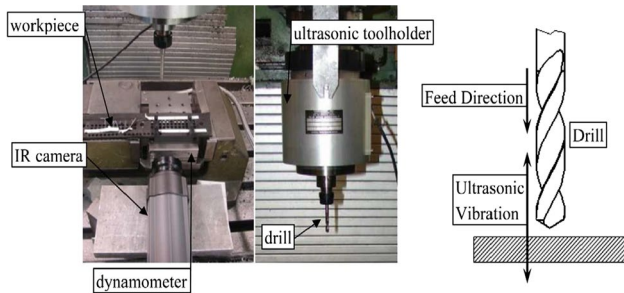
Fig. 3 Experimental setup and application of USV [39]

Table 2 The cutting parameters

Parameters	Values
Rotational speed (rpm)	700, 1000, 1500
Feed rate (mm/rec)	0.01, 0.03, 0.05
Frequency (Hz)	20K, 25.5 K, 30 K

yield stress, hardening module, strain hardening coefficient, strain rate sensitivity and thermal softening. The mechanical and thermal properties of Ti6A14V are shown in Table 1. These parameters are set in the Johnson–Cook model of the DEFORM-3D.

3 Experimental procedure

The picture of the experimental setup is shown in Fig. 3. The ultrasonic vibration devices include an ISO50 tool holder with integrated piezoelectric actuator, ultrasonic generator, etc. Cutting parameters were set based on Table 2, and drilling operations were accomplished in both CD and UAD.

Thrust force measured in the drilling experiments was calculated and compared with the results obtained from the FEA model.

Table 3 shows the comparison of the simulation and experiment thrust force in both CD and UAD by changing of feed rate at spindle speed 1000 rpm for Drill 1. It can be seen that for Drill 1, when the drill feed rate was 0.03 mm/r, the thrust force measured in the experiment was 281 N and the FEM result showed 268 N in CD, whereas was 190 N in the experiment and the FEM result showed 184 N in UAD. The percent errors in results range approximately between 3 and 7% both in CD and in UAD. The percent errors are considered acceptable and can be attributed to the effects of the product of coarse mesh of the work, and it is expected to be reduced by further refining the work mesh in simulation. Therefore, thrust force has a good agreement between the simulation and experiment, which indicates the FEM is accurate.

4 Results and discussion

4.1 Thrust force

Feed rate is one of the major parameters that affect drilling of Ti6A14V. Different pattern was observed for the thrust force with different drill geometry. Figure 4 shows the effect of feed rate and spindle speed on thrust force when drilling Ti6A14V with different drills. It can be seen from Fig. 4a that thrust force went up with the increase in feed rate for three geometrical drills when spindle speed was constant 1000 rpm. It can be attributed to the fact that increase in feed rate causes the increment of uncut chip thickness resulting harder chip formation and larger chip cross-sectional area, which leads to the increment of thrust force to separate the chips from the workpiece. It can be seen from Fig. 4b that thrust force went up with the increase in spindle speed for three geometrical drills when feed rate was constant 0.05 mm/r. This is due to the higher cutting temperature and tool wear progression at higher feed rate. In addition, we can see that the difference among the three geometrical drills becomes smaller and smaller with the spindle speed
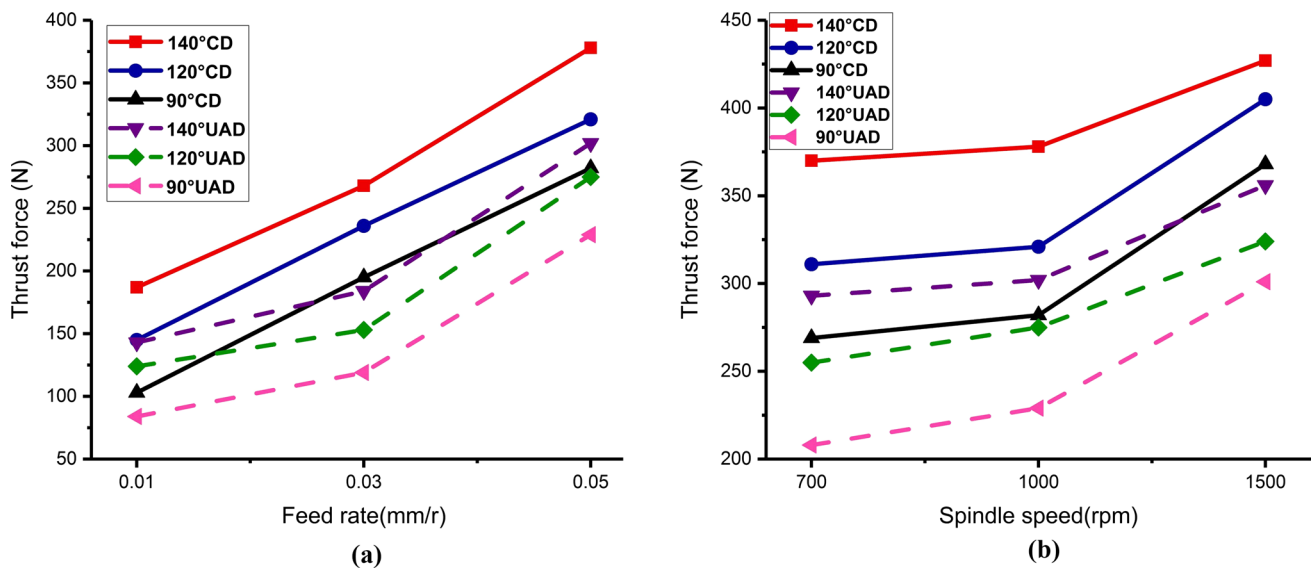
Table 3 Thrust force versus feed rate at spindle speed of 1000 rpm (Drill 1) Simulation results are compared with experimental results [39]

Feed rate (mm/r)	Experiment F_Z (N) in CD	Simulation F_Z (N) in CD	Experiment F_Z (N) in UAD	Simulation F_Z (N) in UAD	Percent errors in CD	Percent errors in UAD
0.01	201	187	150	143	6.97	4.67
0.03	281	268	190	184	4.62	3.16
0.05	400	378	321	302	5.50	5.92

Fig. 4 Influence of feed rate and spindle speed on thrust force when drilling Ti6A14V with different drills

increasing. When the spindle speed goes up to 1500 rpm, the thrust forces of these three drills are very similar. It is observed that the spindle speed also has a positive impact on the thrust force. But the impact is less than that of feed rate. Meanwhile, thrust force in UAD is less than that in CD among three geometrical drills. The thrust force generated by UAD among three geometrical drills at 0.05 mm/r feed rate decreased by 20.10%, 14.30% and 18.80%, respectively. The thrust force generated by UAD among three geometrical drills at 1000 rpm spindle speed decreased by 16.63%, 20.00% and 18.20%, respectively. Pujana et al. [37] have analyzed UAD of Ti6Al4V, observing reductions in thrust forces of 10–20% when using UAD. The reasons could be that the impulsive ultrasonic-separated cutting process of chisel edge and cutting edges at the drill point during UAD greatly improved the removal effect of chip evacuation and lowered the friction effect [12].

It is observed that at the same feed rate, the thrust force increases as the point angle of the drill bit increases both in CD and in UAD. The reason is that as the point angle of the drill bit increases, the increase in the cutting material leads to an increase in the cutting resistance, which eventually results in an increase in the thrust force. In general, the UAD processing can reduce the thrust force, and the thrust force gradually decreases with the decrease in point angle. In addition, the thrust force of the Drill 1 is the highest.

Figure 5 shows the effect of vibration frequency on thrust force when drilling Ti6A14V with different drills. It can be clearly seen from the figure that the thrust force generated when the vibration is increased is lower than that without vibration, and thrust force decrease with the increase in vibration frequency for three geometrical drills
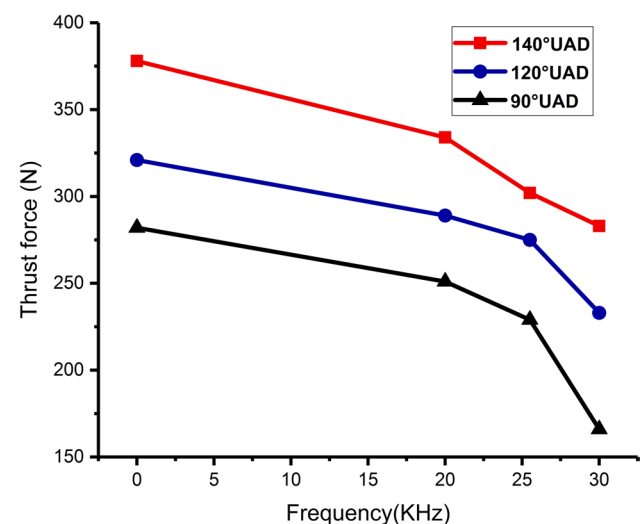

Fig. 5 Influence of frequency on thrust force when drilling Ti6A14V with different drills

when feed rate was constant 0.05 mm/r. To be specific, for Drill 1, thrust force decreased by 25.31% when the vibration frequency increased from 0 to 30 KHz; for Drill 2, thrust force decreased by 27.41%; for Drill 3, thrust force decreased by 41.13%. In addition, the thrust force of the Drill 3 is the lowest. This reduction of thrust force definitely enhances system stability and, as a consequence, improves hole quality. It is observed that the vibration frequency has a positive impact on the thrust force for Ti6A14V.

4.2 The distribution of temperature

Temperature is one of the key factors in improving the productivity of advanced engineering materials. Analysis of the temperature distribution is essential to better understand the drilling process. Figure 6 shows the distribution of temperature in CD and UAD processes for Drill 1. It can be seen that three different times started from 0.025 s up to 0.0715 s in CD with almost the relatively stable temperature, as shown in Fig. 6a, whereas UAD simulation has been classified into six stages in one harmonic cycle started from 0.005 s and ended at 0.167 s, as shown in Fig. 6b. In stage 1, the drill tool approaches the workpiece and touches the work surface and, in stage 2, continues penetrating into the workpiece until maximum temperature occurs in stage 3. In stage 4, the drill tool starts to detract

from the workpiece and the temperature starts to go down. In stage 5, this action continues and the drill tool partially separates from the workpiece. At the last stage, the drill tool fully disengages the workpiece and temperature is reduced to a minimum. This cycle is repeated until the end of drilling.

Figure 7 shows the distribution of temperature in CD and UAD for three different drills. It can be seen that the maximum temperature came mainly from the cutting zone between the cutting edges of drill point and the contact area of the front cutter face in CD, whereas occurred in the chip in UAD. It can be attributed to the fact that the cutting temperature of the titanium alloy drilling process is mainly from the cutting edge of the tool drill tip and the bottom of the hole. Due to the periodic separation between the chisel edge and the cutting edge and the material of the
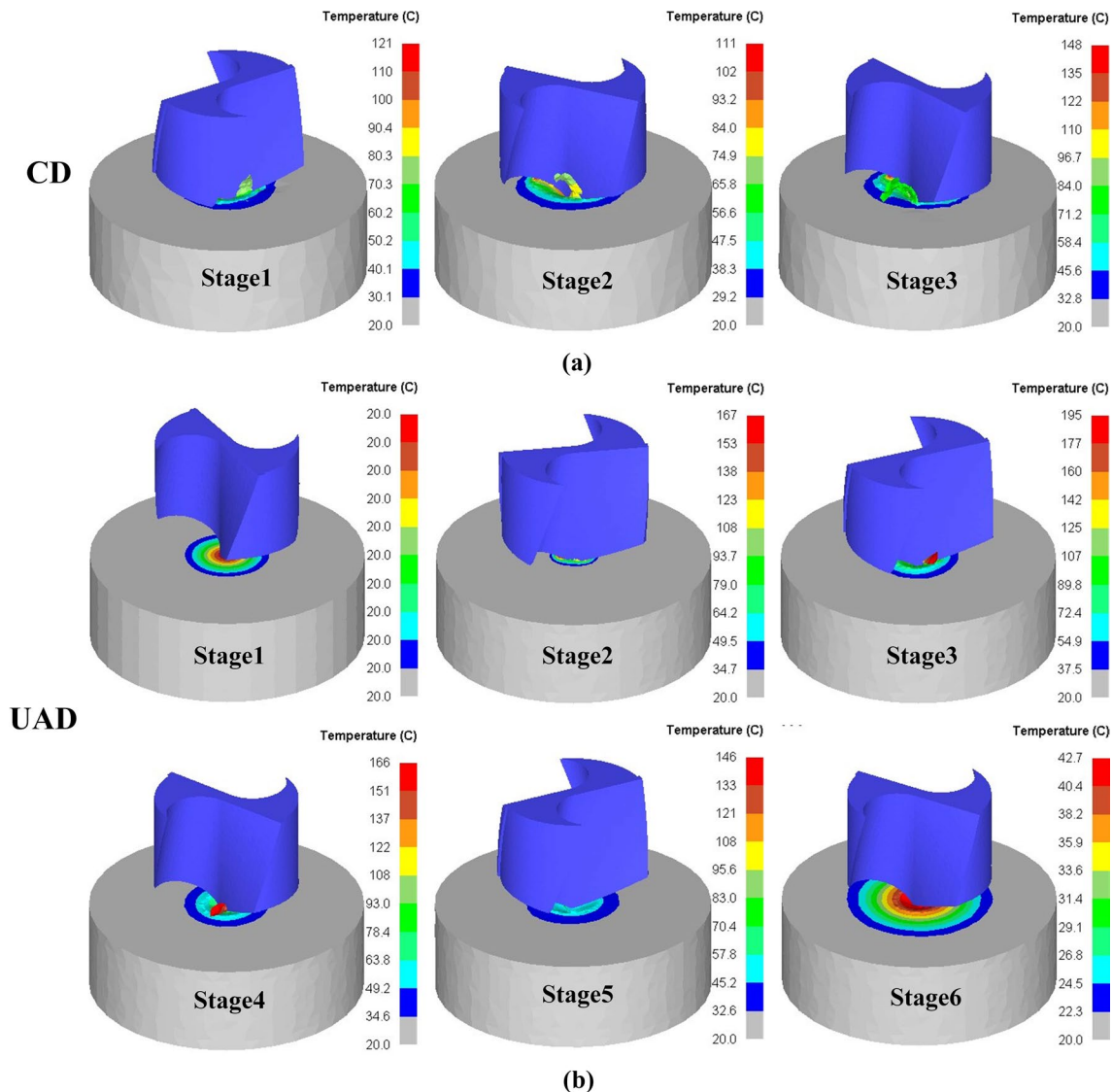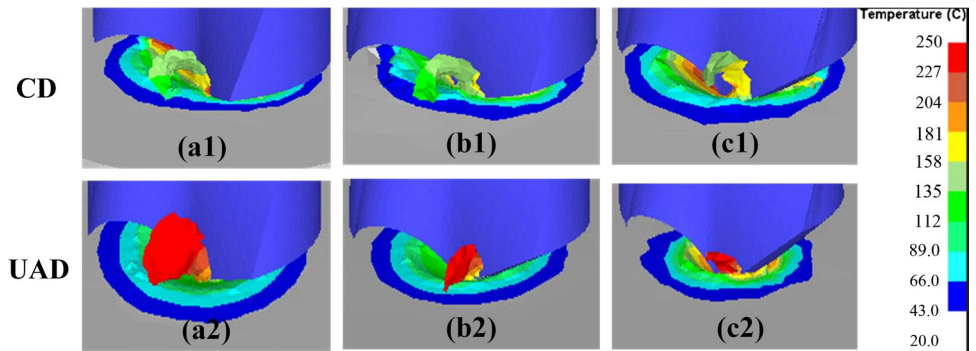

Fig. 6 The distribution of temperature in CD (**a**) and UAD (**b**) processes for Drill 1. Spindle speed 1000 rpm and feed rate 0.03 mm/r

Fig. 7 The distribution of temperature in CD [**a1** Drill 1; **b1** Drill 2; **c1** Drill 3] and UAD [**a2** Drill 1; **b2** Drill 2; **c2** Drill 3] for three different drills. Spindle speed 1000 rpm and feed rate 0.03 mm/r

hole bottom in the UAD process, the cutting heat of the UAD is mainly concentrated on the chips.

Figure 8 shows the effect of feed rate and spindle speed on temperature when drilling Ti6A14V with different drills. It can be seen from Fig. 8 that temperature went up with the increase in feed rate and spindle speed for three geometrical drills.

Meanwhile, temperature in UAD is less than that in CD among three geometrical drills. The temperature generated by UAD among three geometrical drills at 0.05 mm/r feed rate decreased by 27.90%, 30.00% and 31.10%, respectively. The temperature generated by UAD among three geometrical drills at 1000 rpm spindle speed decreased by 7.74%, 9.72% and 12.91%, respectively. The reasons could be that the drill tool separates from the chip within each cycle in UAD, and such an intermittent movement leads to a reduction in the total time of heat transfer between the drill tool and chip.

At the same time, the cutting tool can get a certain degree of cooling in the uncut stage because of the intermittent

cutting characteristics of vibration drilling, and the cutting temperature will decrease eventually. The size of the chips is small, and it is easy to discharge quickly with the spiral groove, while taking away a lot of cutting heat. Therefore, the temperatures of UAD could be decreased significantly compared with CD.

It is observed that the temperature increases as the point angle of the drill bit increases. It can be attributed to the fact that with the increase in the point angle, the cutting edge of the drill bit will become thinner, the outer edge of the cutting edge becomes smaller, the volume of the drill capable of dissipating heat is reduced, and the heat dissipation is deteriorated, which leads to the difficulty in diverging the cutting heat when drilling a titanium alloy material having poor thermal conductivity, causing the temperature to rise.

Figure 9 shows the effect of vibration frequency on temperature when drilling Ti6A14V with different drills. It can be seen that temperature decreases with the increase in vibration frequency for three geometrical drills when feed rate was constant 0.05 mm/r. To be specific, for Drill
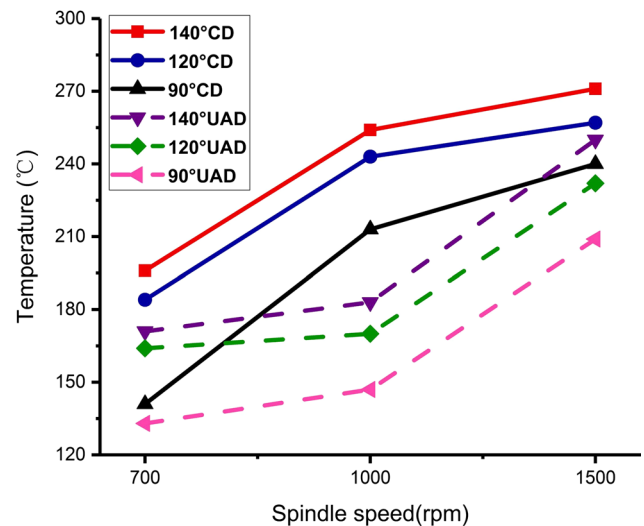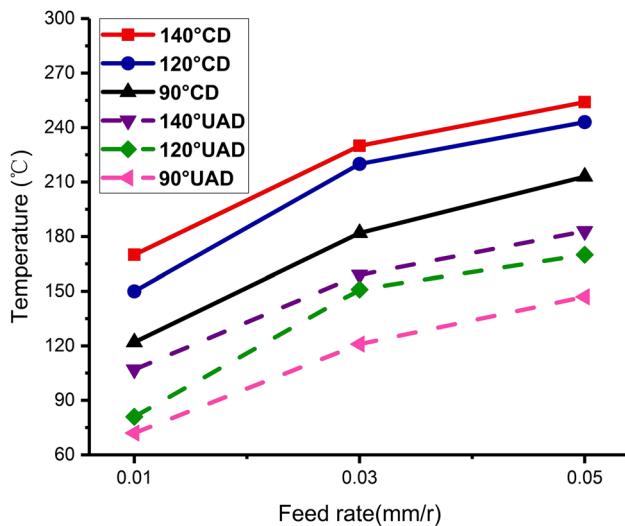

Fig. 8 Influence of feed rate and spindle speed on temperature when drilling Ti6A14V with different drills
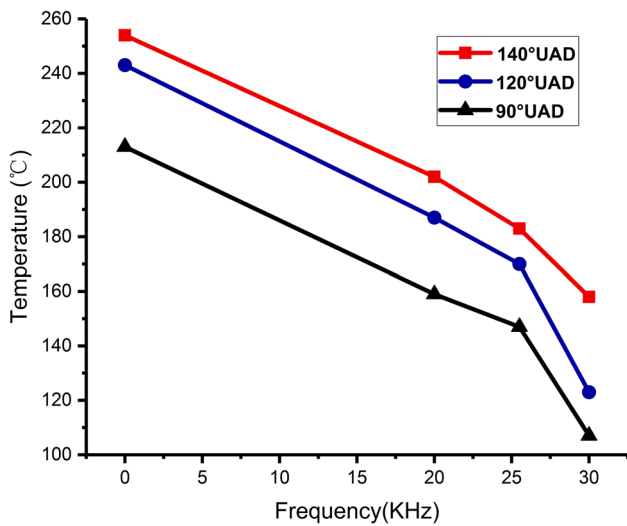
Fig. 9 Influence of frequency on temperature when drilling Ti6A14V with different drills

1, temperature decreased by 37.79% when the vibration frequency increased from 0 to 30 KHz. In addition, the temperature of the Drill 3 is the lowest. It is observed that the vibration frequency has a positive impact on the temperature for Ti6A14V.

4.3 The distribution of effective stresses

Figure 10 shows the distribution of effective stresses in CD and UAD for three different drills when feed rate was 0.03 mm/r and spindle speed was 1000 rpm. It can be seen that the maximum effective stress was largest for Drill 2 both in CD and in UAD, as shown in Fig. 10b1, b2. The high stress is always located at primary shear zone and chisel edges squeezing zone and follows the moving of these two zones both in CD and in UAD. In particular the maximum effective stress appears at the intersection of lips and margins, where the work material is undergoing higher equivalent strain and lower hydrostatic pressure than that at other places of the primary shear zone. Meanwhile, the maximum effective stress of the UAD is lower than CD. It can be attributed to the fact that the thousands of harmonic cycles that occur repeatedly in UAD results in significantly less stress distribution due to less contact and meshing time between drill bit with workpiece and chip.

Figure 11 shows the distribution of effective stresses in CD and UAD at different feed rates for Drill 1 when spindle speed was constant at 1000 rpm. It can be seen that the maximum effective stress increases with the feed rate from 0.01 to 0.05 mm/r due to the increasing of cutting thickness both in CD and in UAD, as shown in Fig. 11a1–c1, a2–c2.

Figure 12 shows the distribution of effective stresses in CD and UAD at different spindle speeds for Drill 1 when

Fig. 10 The distribution of effective stresses in CD [**a1** Drill 1; **b1** Drill 2; **c1** Drill 3] and UAD [**a2** Drill 1; **b2** Drill 2; **c2** Drill 3] for three different drills
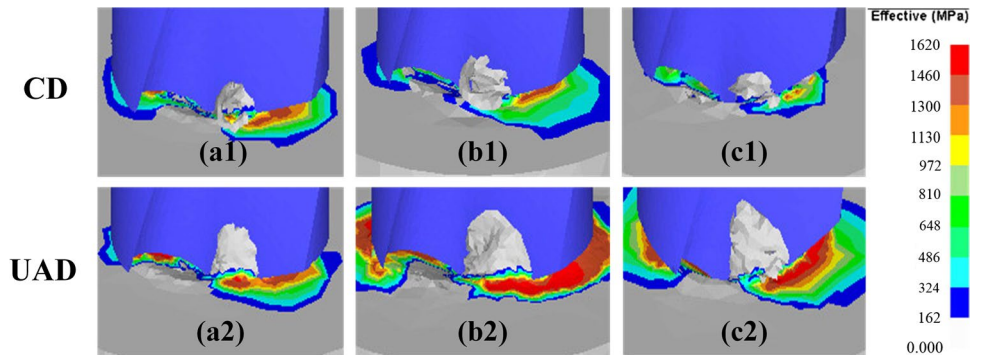

Fig. 11 The distribution of effective stresses in CD [**a1** 0.01 mm/r; **b1** 0.03 mm/r; **c1** 0.05 mm/r] and UAD [**a2** 0.01 mm/r; **b2** 0.03 mm/r; **c2** 0.05 mm/r] at different feed rates for Drill 1
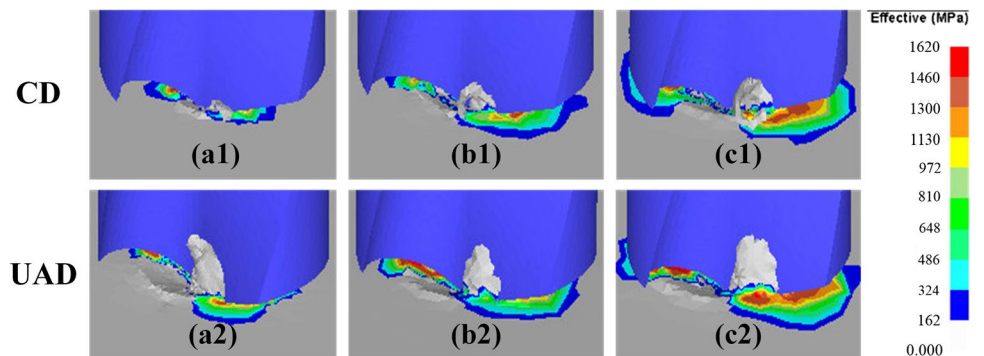
Fig. 12 The distribution of effective stresses in CD [**a1** 700 rpm; **b1** 1000 rpm; **c1** 1500 rpm] and UAD [**a2** 700 rpm; **b2** 1000 rpm; **c2** 1500 rpm] at different spindle speeds for Drill 1
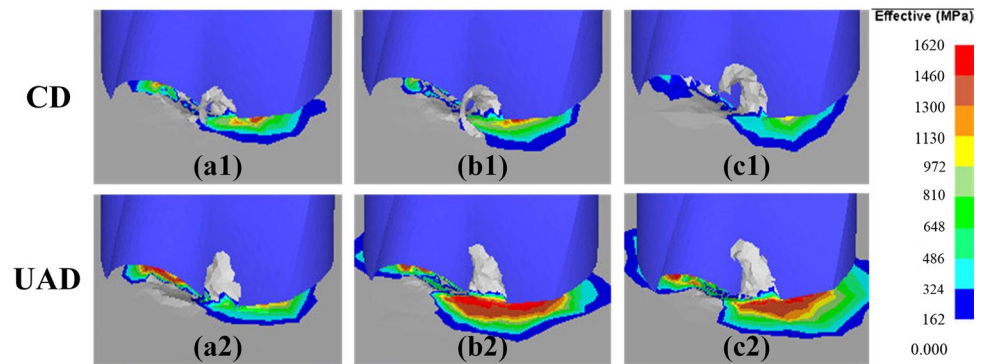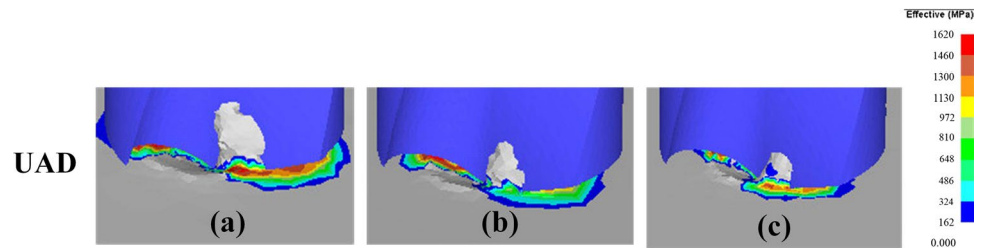

Fig. 13 The distribution of effective stresses in UAD **a** 20 KHz; **b** 25.5 KHz; **c** 30 KHz at different frequencies for Drill 1

feed rate was constant 0.03 mm/r. It can be seen that the maximum effective stress was almost identical in CD, so the spindle speed has little influence on the effective stress. But the maximum effective stress was lowest when spindle speed was 700 rpm in UAD, as shown in Fig. 12a2.

Figure 13 shows the distribution of effective stresses in CD and UAD at different frequencies for Drill 1. It can be seen that the maximum effective stress was lowest when frequency was 25.5 KHz, as shown in Fig. 13b.

4.4 Chip morphology

The chip morphology produced during the drilling process is an important problem because it plays an important role in the safety of the operator, the temperature of the processing area and the tool life. Figure 14 shows experimental and FEM results of chip morphology with Drill 1 in CD. It can be seen that the simulated chip thickness and the chip type highly correspond to the actual chip in experiment. Therefore, the experimental and simulation results are in a good agreement.

The chip morphology could be classified into two main categories comprised of continuous and discontinuous chips. In the process of chip formation, deformation and crimping will occur. The smaller the chip thickness, the bigger the deformation and crimping will be, which will generate chip breaking effect. Figure 15 shows the chip morphology in CD and UAD for three different drills when feed rate was 0.05 mm/r and spindle speed was 700 rpm. It can be seen that the chip thickness was thinnest for Drill 2 both in CD and in UAD, as shown in Fig. 15b1, b2. The chip morphology was
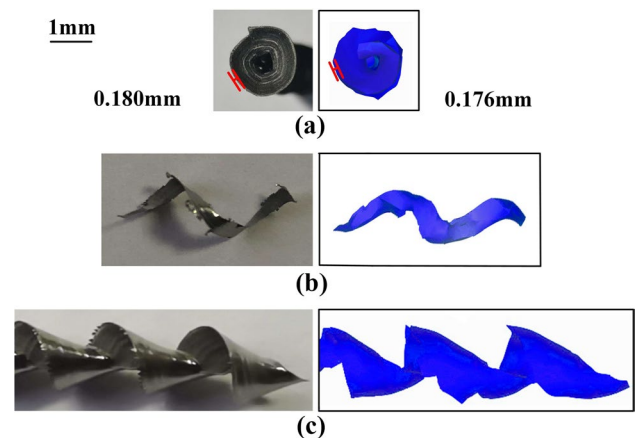

Fig. 14 Comparison of chip morphology in CD for Drill 1 between experiment and simulation, feed rate 0.03 mm/r, and spindle speed 700 rpm

the spiral continuous chip due to the unseparated continuous drilling process and big continuous extrusion force in CD, whereas was segmental discontinuous chip because the intermittent movement of drill impacts the chip in UAD.

Meanwhile, the damage in UAD is distinctly larger than that in CD in the same drilling time and drilling parameters. The chip thickness in UAD was obviously thinner than that in CD. The reason is that UAD is pulse drilling, in which part of the reinforcing particles at the shear interface are cut off due to the impact of ultrasonic wave. The intermittent contact between the tool and the workpiece, at the moment of disengagement, the bottom layer of the chip will form an
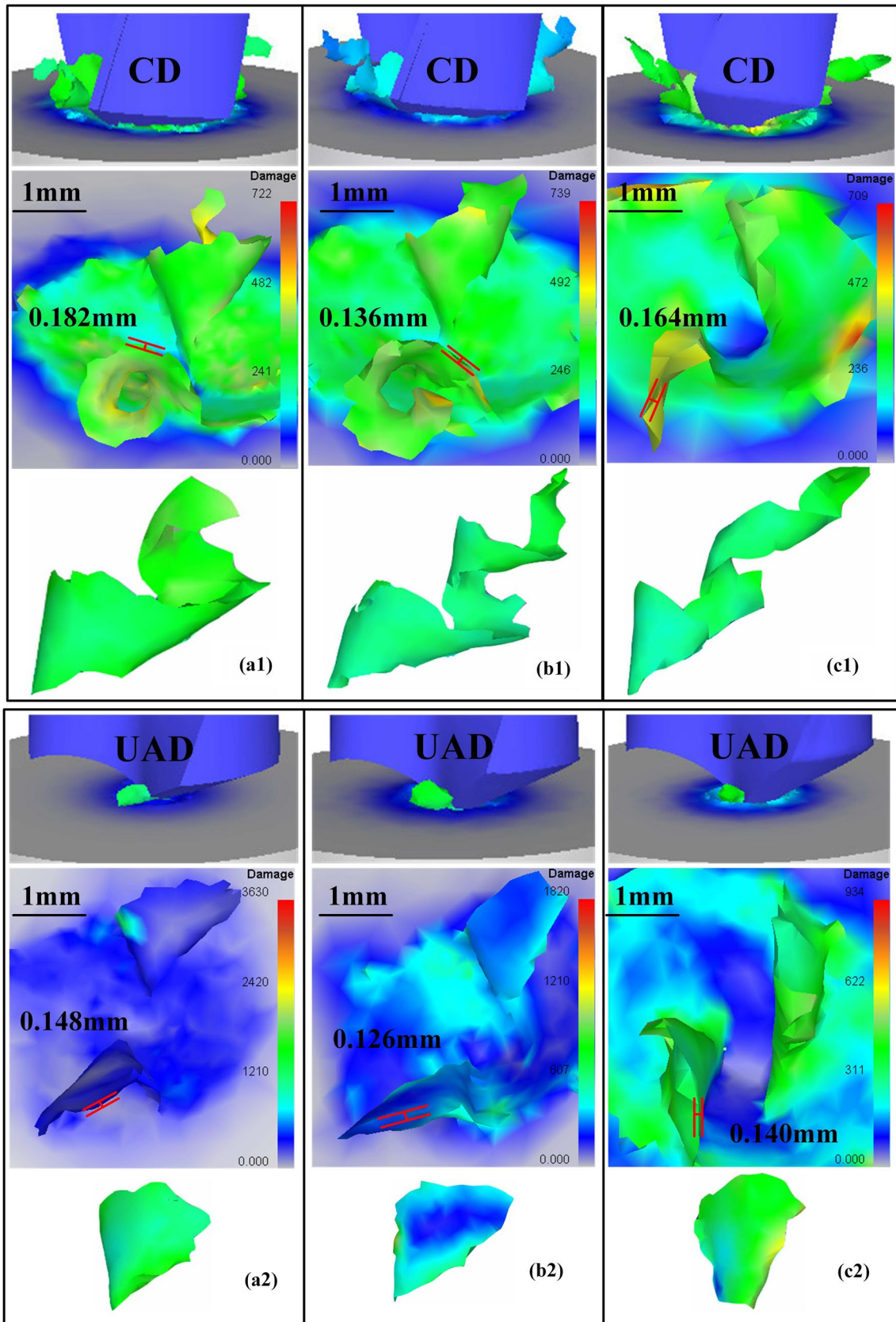
Fig. 15 The chip morphology in CD [**a1** Drill 1; **b1** Drill 2; **c1** Drill 3] and UAD [**a2** Drill 1; **b2** Drill 2; **c2** Drill 3] for three different drills

oxide layer to prevent the bond bottom layer from bonding with the tool rake face, thereby reducing the friction coefficient between tool and chip, and increasing the shear angle. The chip deformation coefficient increases accordingly.

Figure 16 shows the chip morphology in CD and UAD at different feed rates for Drill 1 when spindle speed was constant 700 rpm. It can be seen that chip thickness went up with the increase in feed rate both in CD and in UAD. The reason is that as the feed rate increases, the material to be cut increases, resulting in the increase in chip thickness.

Figure 17 shows the chip morphology in CD and UAD at different spindle speeds for Drill 1 when feed rate was constant 0.03 mm/r. It can be seen that the chip thickness of UAD is also lower than CD. In addition, the chip thickness was thinnest when spindle speed was 1000 rpm both in CD and in UAD, as shown in Fig. 17b1, b2. Therefore, 1000 rpm spindle speed has a positive impact on the chip breakability.

Figure 18 shows the chip morphology in CD and UAD at different frequencies for Drill 1. It can be seen that the chip thickness was thinnest when frequency was 30 KHz, as shown in Fig. 18c. It is observed that the vibration frequency has a positive impact on the chip thickness for drilling Ti6A14V.
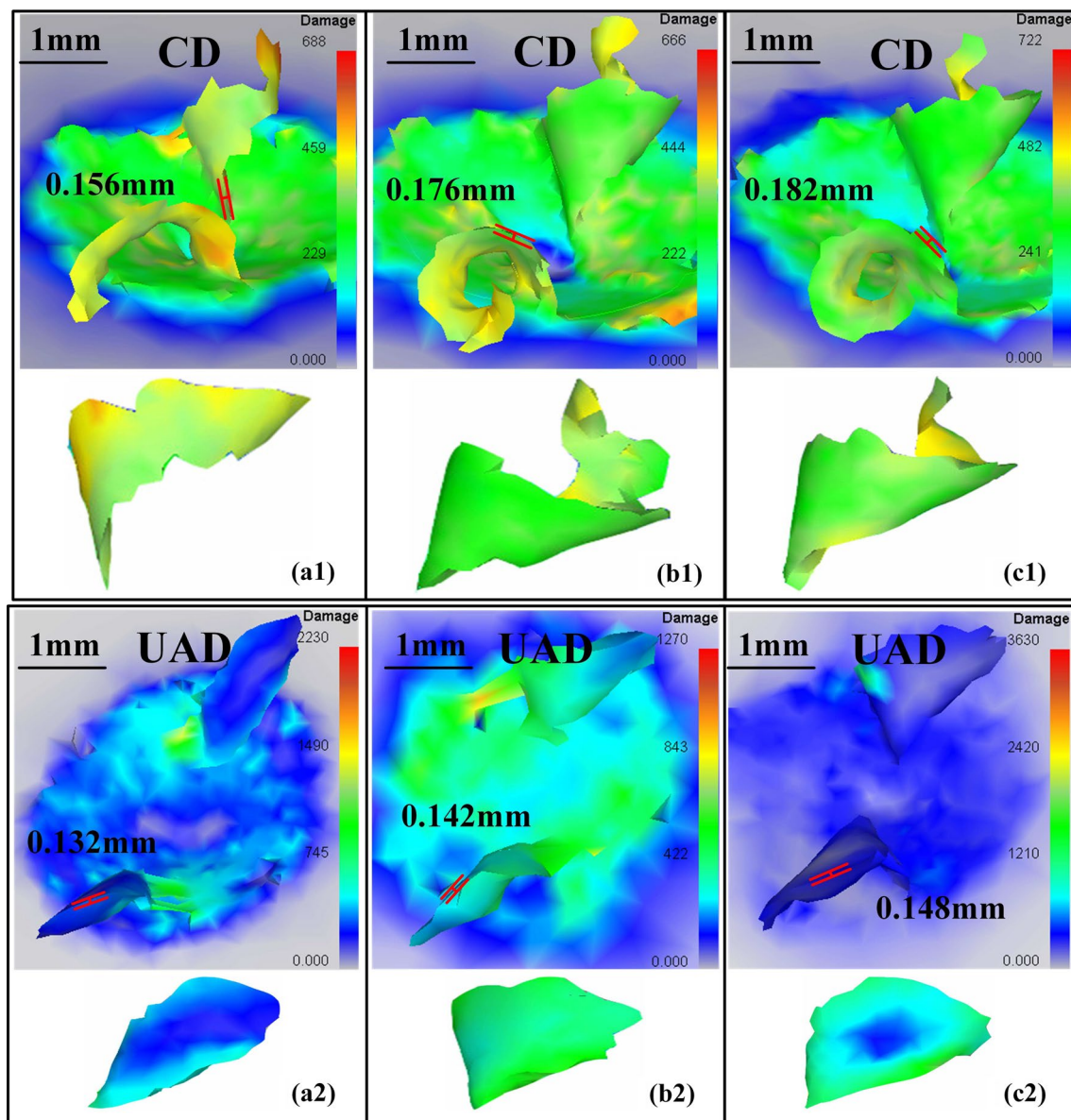

Fig. 16 The chip morphology in CD [**a1** 0.01 mm/r; **b1** 0.03 mm/r; **c1** 0.05 mm/r] and UAD [**a2** 0.01 mm/r; **b2** 0.03 mm/r; **c2** 0.05 mm/r] at different feed rates for Drill 1
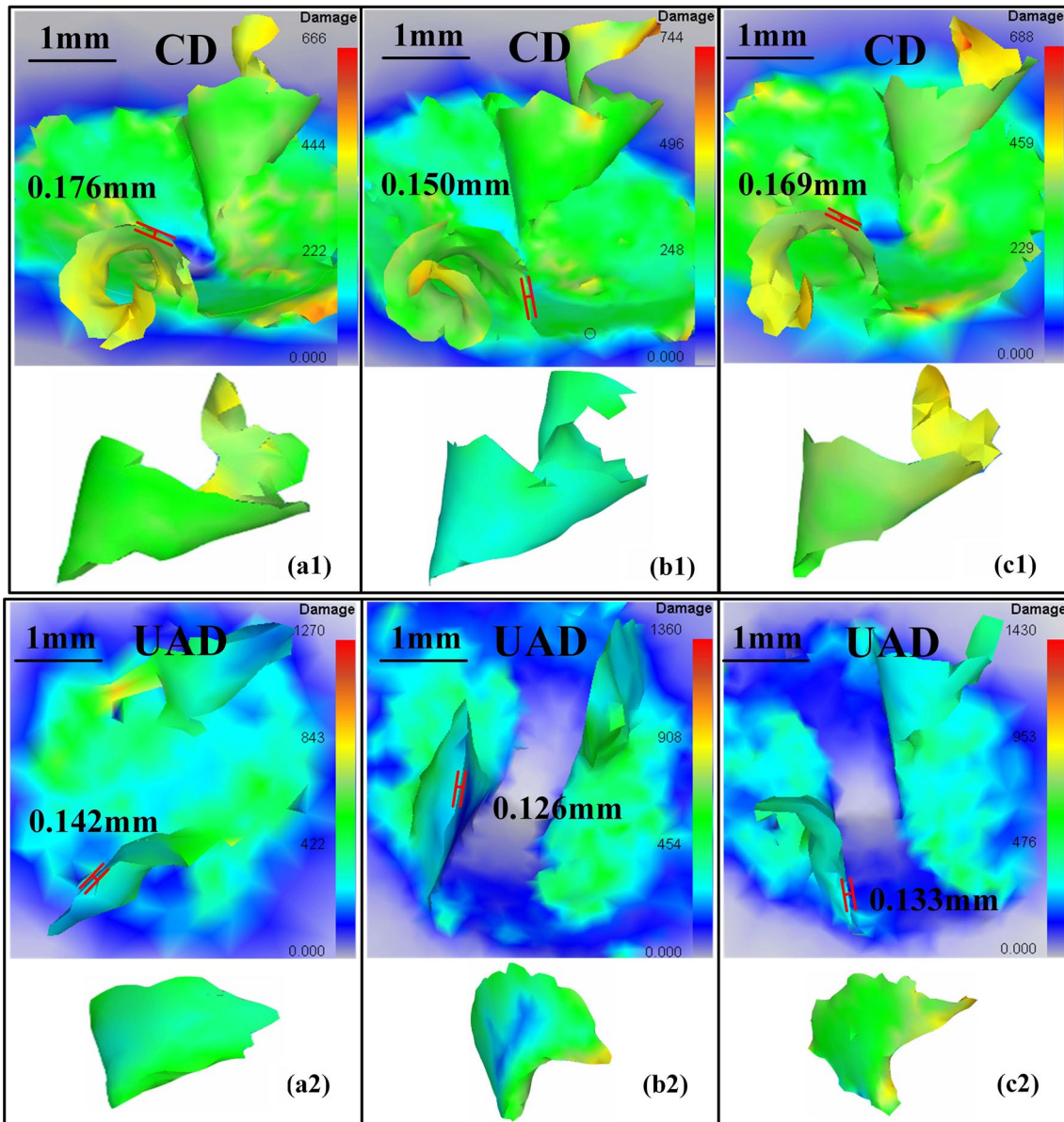
Fig. 17 The chip morphology in CD [**a1** 700 rpm; **b1** 1000 rpm; **c1** 1500 rpm] and UAD [**a2** 700 rpm; **b2** 1000 rpm; **c2** 1500 rpm] at different spindle speeds for Drill 1

5 Conclusions

In this paper, three different point angle drills are designed to investigate their machining characteristics during drilling Ti6Al4V in the finite element simulation. The effect of tool geometries, feed rates, spindle speeds and frequencies on thrust force, effective stresses, temperature and chip morphology have been analyzed and compared using DEFORM 3D both in CD and in UAD. From this research, the following conclusions can be drawn.

1. The percent errors in results range approximately between 3 and 7% both in CD and in UAD. Therefore, thrust force has a good agreement between the simulation and experiment, which indicates the FEM is accurate.

2. Compared with CD, the thrust force decreased by 13–22% on average in UAD, which improves the drilling capacity. The thrust force increases as the point angle of the drill bit increases both in CD and in UAD due to the increase in the cutting resistance.
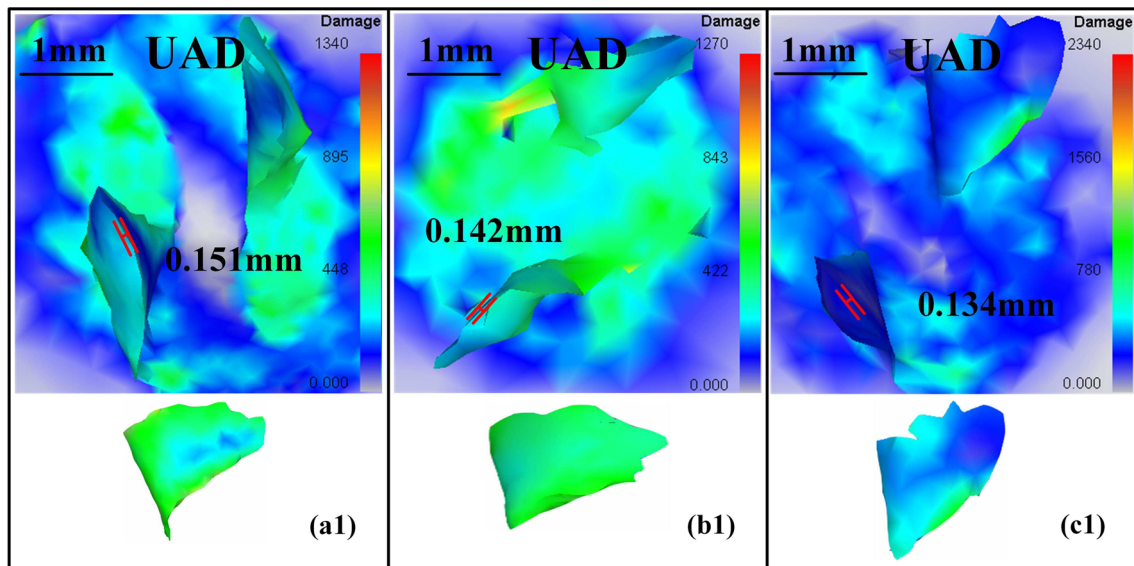
Fig. 18 The chip morphology in UAD **a** 20 KHz; **b** 25.5 KHz; **c** 30 KHz at different frequencies for Drill 1

3. The maximum temperature came mainly from the cutting zone between the cutting edges of drill point and the contact area of the front cutter face in CD, whereas occurred in the chip in UAD. Compared with CD, the temperature decreased by 7–15% on average in UAD due to an intermittent movement between the drill tool and chip. The maximum effective stress of the UAD is lower than CD, which can reduce tool wear. The maximum effective stress was lowest for Drill 1 in UAD.

4. The chip morphology was the spiral continuous chip in CD, whereas was segmental discontinuous chip in UAD. Compared with CD, UAD has the excellent effects of chip breaking. Drill 2 is more conducive to chip breaking both in CD and in UAD. Point angle of the drill has high importance in effecting chip breaking when drilling Ti6Al4V.

References

1. Iyer R, Koshy P, Ng E (2007) Helical milling: an enabling technology for hard machining precision holes in AISI D2 tool steel. Int J Mach Tools Manuf 47(2):205–210

2. Tsao C (2008) Experimental study of drilling composite materials with step-core drill. Mater Des 29:1740–1744

3. Ni C, Zhu LD, Liu CF, Yang ZC (2018) Analytical modeling of tool-workpiece contact rate and experimental study in ultrasonic vibration-assisted milling of Ti-6Al-4V. Int J Mech Sci 142–143:97–111

4. Zhang L, Ji RQ, Fu YF, Qi H, Li HN (2020) Viboon Tangwarodomnukun, Investigation on particle motions and resultant impact erosion on quartz crystals by the micro-particle laden waterjet and airjet. Powder Technol 360:452–461

5. Zhu ZJ, Sui SC, Sun J, Li JF, Li YL (2017) Investigation on performance characteristics in drilling of Ti6Al4V alloy. Int J Adv Manuf Technol 93:651–660

6. Li HN, Yang Y, Zhao YJ, Zhang ZL, Zhu WQ, Wang WL, Qi H (2019) On the periodicity of fixed-abrasive planetary lapping based on a generic model. J Manuf Process 44:271–287

7. Qi H, Cheng ZC, Cai DH, Yin LZ, Wang ZW, Wen DH (2018) Experimental study on the improvement of surface integrity of tungsten steel using acoustic levitation polishing. J Mater Process Technol 259:361–367

8. Wang YG, Li CH, Zhang YB, Yang M, Li BK, Jia DZ, Hou YL, Mao C (2016) Experimental evaluation of the lubrication properties of the wheel/workpiece interface in minimum quantity lubrication (MQL) grinding using different types of vegetable oils. J Clean Prod 127:487–499

9. Glaa N, Mehdi Kamel, Zitoune R (2018) Numerical modeling and experimental analysis of thrust cutting force and torque in drilling process of titanium alloy Ti6Al4V. Int J Adv Manuf Technol 96:2815–2824

10. Armendia M, Garay A, Iriatre LM, Arrazola PJ (2010) Comparison of the machinabilities of Ti6Al4V and TIMETAL-54 M using uncoated WC-Co tools. J Mater Process Technol 210:197–203

11. Islam C, Lazoglu I, Altintas Y (2016) A three-dimensional transient thermal model for machining. J Manuf Sci Eng 138:21003

12. Abdelhafeez AM, Soo SL, Aspinwall DK, Dowson A, Arnold D (2015) Burr formation and hole quality when drilling titanium and aluminium alloys. Procedia CIRP 37:230–235

13. Pawar OA, Gaikhe YS, Tewari A, Sundaram R, Joshi SS (2015) Analysis of hole quality in drilling GLARE fiber metal laminates. Compos Struct 123:350–365

14. Rahim EA, Sasahara H (2011) A study of the effect of palm oil as mql lubricant on high speed drilling of titanium alloys. Tribol Int 44:309–317

15. Liu K, Li J, Sun J, Zhu Z, Meng H (2018) Investigation on chip morphology and properties in drilling aluminum and titanium stack with double cone drill. Int J Adv Manuf Technol 94:47–56

16. Zhu ZJ, Guo K, Sun J (2018) Evaluation of novel tool geometries in dry drilling aluminium 2024-T351/ titanium Ti6Al4V stack. J Mater Process Technol 259:270–281

17. Zhang YB, Li CH, Ji HJ, Yang XH, Yang M, Jia DZ, Zhang XP, Li RZ, Wang J (2017) Analysis of grinding mechanics and improved predictive force model based on material-removal and plastic-stacking mechanisms. Int J Mach Tools Manuf 122:81–97

18. Kuo CL, Soo SL, Aspinwall DK, Carr C (2018) Development of single step drilling technology for multilayer metallic-composite stack using uncoated and PVD coated carbide tools. J Manuf Process 31:286–300

19. Chang SS, Bone GM (2009) Thrust force model for vibration-assisted drilling of aluminum 6061CT6. Int J Mach Tools Manuf 49:1070–1076

20. Pujana J, Rivero A, Celaya A (2009) Analysis of ultrasonic-assisted drilling of Ti6Al4V. Int J Mach Tools Manuf 49:500–508

21. Ni C, Zhu L (2019) Investigation on machining characteristics of TC4 alloy by simultaneous application of ultrasonic vibration assisted milling (UVAM) and economical-environmental MQL technology. J Mater Process Technol. https://doi.org/10.1016/j.jmatprotec.2019

22. Makhdum F, Jennings LT, Roy A, Silberschmidt VV (2012) Cutting forces in ultrasonically assisted drilling of carbon fibre-reinforced plastics. J Phys Conf Ser 382:28–31

23. Lotfi M, Amini S (2017) Experimental and numerical study of ultrasonically-assisted drilling. Ultrasonics 75:185–193

24. Yang M, Li CH, Zhang YB, Jia DZ, Zhang XP, Hou YL, Li RZ, Wang J (2017) Maximum undeformed equivalent chip thickness for ductile–brittle transition of zirconia ceramics under different lubrication conditions. Int J Mach Tools Manuf 122:55–65

25. Barani A, Amini S, Paktinat H, Tehrani AF (2014) Built-up edge investigation in vibration drilling of Al2024-T6. Ultrasonics 54:1300–1310

26. Amini S, Tehrani AF, Barani A, Paktinat H (2012) Vibration drilling process on Al2024. Adv Mater Res 445:79–83

27. Jia Z, Fu R, Niu B, Qian B, Bai Y, Wang F (2016) Novel drill structure for damage reduction in drilling CFRP composites. Int J Mach Tools Manuf 110:55–65

28. Majeed A, Iqbal A, Lv JX (2018) Enhancement of tool life in drilling of hardened AISI 4340 steel using 3D FEM modeling. Int J Adv Manuf Technol 95:1875–1889

29. Muhammad R, Ahmed N, Shariff YM, Silbers VV (2012) Finite-element analysis of forces in drilling of Ti-alloys at elevated temperature. Solid State Phenom 188:250–255

30. Wu HB, Jia ZX, Zhang XC, Liu G (2012) Study on simulation and experiment of drilling for titanium alloys. Mater Sci Forum 704:657–663

31. Marasi A (2013) Modeling the effects of cutting parameters on the main cutting force of Ti6Al4V alloy by using hybrid approach. Int J Adv Eng Appl 2:6–14

32. Ahmed N (2014) Effect of changing drilling parameters on thrust force and torque. Middle East J Sci Res 21:347–352

33. Chatterjee S, Mahapatra SS, Abhishek K (2016) Simulation and optimization of machining parameters in the drilling of titanium alloys. Simul Model Pract Theory 62:31–48

34. Wu X, Li L, He N, Zhao GL, Shen JY (2019) Laser induced oxidation of cemented carbide during micro milling. Ceram Int 45(12):15156–15163

35. Attanasio A, Faini F, Outeiro JC (2017) FEM simulation of tool wear in drilling. Procedia CIRP 58:440–444

36. Ucun I (2016) 3D finite element modeling of the drilling process of Al7075-T6 alloy and experimental validation. J Mech Sci Technol 30:1843–1850

37. Phadnis VA, Roy A, Silberschmidt VV (2013) A finite element model of ultrasonically assisted drilling in carbon/epoxy composites. Procedia CIRP 8:141–146

38. Paktinat H, Amini S (2017) Ultrasonic assistance in drilling: FEM analysis and experimental approaches. Int J Adv Manuf Technol 92:2653–2665

39. Sanda A, Arriola I, Navas VG, Bengoetxea I, Gonzalo O (2016) Ultrasonically assisted drilling of carbon fibre reinforced plastics and Ti6Al4V. J Manuf Process 22:169–176